MICROSTRUCTURAL CHARACTERIZATION OF LASER POWDER BED FUSION (L-PBF) ADDITIVELY MANUFACTURED INCONEL 718 FOR AEROSPACE APPLICATION

A. Doris^{1,3}, L. Trujillo^{1,3}, Dana Godinez^{1,3}, E. Arrieta^{1,2}, R.B. Wicker^{1,2}, P. Gradl⁴, and F. Medina^{1,2}

¹ W.M. Keck Center for 3D Innovation, The University of Texas at El Paso, El Paso, TX 79968, USA

² Department of Aerospace and Mechanical Engineering, The University of Texas at El Paso, TX 79968, USA

³ Department of Metallurgical, Materials and Biomedical Engineering, The University of Texas at El Paso, TX 79968. USA

⁴ NASA Marshall Space Flight Center, Huntsville, Al, 35812, USA

Keywords: Additive Manufacturing, Laser Powder Bed Fusion (L-PBF); Inconel 718; Microstructural Characterization.

ABSTRACT

Alloy 718 (Inconel 718) is used for aerospace applications because of its excellent corrosion resistance and mechanical properties. This alloy is particularly applicable in manufacturing components subjected to high temperatures in rocket engines, aero-engines, and gas turbines. Properties for this alloy when processing on systems from similar and different Laser Powder Bed Fusion (L-PBF) machines provide subtle differences due to process parameters, feedstock, and machine configurations. A series of sixteen L-PBF AM Inconel 718 geometric feature build plates have been evaluated for microstructure using optical microscopy. This study presents the details of the microstructure analysis concerning geometry and different machine platforms. Microstructural investigations of these samples included average grain width measurement for all the X-Y and Y-Z build layers and are accompanied by process parameters and powder characterization. The present work concludes with a discussion on the importance of captured differences among builds to understand the practical limitations among AM platforms.

1 Introduction

Metal additive manufacturing (AM) has shown evolutionary technical and programmatic development exceeding traditional manufacturing processes for aerospace and various industrial applications. AM has enabled designers to make extensively complex features while reducing the number of parts in an overall assembly [1]. The intriguing aspects of AM include a reduction in cost and lead times, design optimization, the rapid development of prototypes, mass reduction, and enabling the use of traditionally challenging materials like novel alloys [1], [2]. Laser Powder Bed Fusion (L-PBF) is one of the most utilized AM processes associated with using the laser beam to melt metal powder feedstock selectively. In processing, predetermined build toolpath and parameters are defined from CAD models to melt each layer, creating an entire part. An inert gas (argon or nitrogen) environment is maintained for reactivity prevention [3]. Several focuses of ongoing research for L-PBF have included process control, machine parameters, feedstock, post-processing operations, geometric tolerances, and resulting microstructure [4]. The layer-by-layer

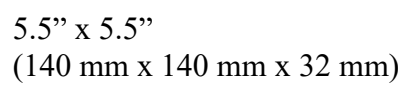
^{*} Corresponding author (adoris@miners.utep.edu)

material melting in L-PBF enables the production of complex and lightweight structures like thin walls. [6] A previous study by Gradl et al. discussed several ASTM/ ISO standardized and custom features, geometric tolerances, process capability, and reproducibility of sixteen L-PBF additively manufactured Inconel 718 build plates from different machine configurations [2]. The present study focuses on the microstructural evaluations, including microscopic images and grain width measurements of one of those features, vertical thin walls with varying thicknesses from 0.1 to 2 mm. Inconel 718 is a nickel-based superalloy broadly used in aerospace, energy, and automotive industries due to its corrosion resistance, high yield strength, and creep resistance at extreme temperatures [7]. Proper characterization and determining the exact geometry that is used in parts is critical in assessing the performance and quality of the L-PBF additively manufactured Inconel 718 product, as thickness can have an impact based on varying thermal history. This study aims to provide a comparative outline of the microstructure of etched vertical thin wall samples from sixteen different builds across fifteen machines using Inconel 718.

2 Materials and Methods

2.1 Feature build plate Description

Sixteen L-PBF AM Inconel 718 build plate artifacts were received in fully heat-treated including Stress Relief, Hot Isostatic Pressing, Solution, and Aged (SR, HIP, SOL, AGE) conditions. The build plates and geometric features underwent stress relieving at 1066 °C for 90 min and slow cooling in the furnace according to ASTM F3055-14a. The HIP was completed per standard ASTM 3301-18a and the solution and 2-step aging per AMS 5664. The nominal dimensions of the feature build plate were 140 mm in X-orientation, 140 mm in Y-orientation, and 32 mm in Zheight. The feature build plate volume was 143 cm³, associated with a surface area of 722 cm² and a mass of 1.34 kg. The geometric features include varying angle walls; X- and Y- distances; horizontal holes; and vertical features, including round holes, concentric hollow cylinders, protruding cylinders, thin wall thickness, square channels, freeform surface, and slots. The base layer of Inconel 718 containing all the features is 3.81 mm in thickness [1]. The thin vertical walls being studied in this paper ranged from 0.10 to 2.0 mm in width. Not all the walls were built successfully, especially the thinnest wall (no.1) wall at 0.1 mm for most of the built plates failed completely, partially built, or thicker than designed. Only four machine configurations appeared to successfully build the 0.10 mm wall, including plates 7, 10, 11, and 12, but thicker than desired. The smallest two wall widths, 0.10 mm and 0.20 mm in thickness, were subjected to complete failure or curling in most cases. An isometric view of the sample build plate design with all the geometric features has been shown in Fig 1. Information from service vendors regarding machine configurations and build parameters have been listed in Table 1, which was provided in the previous study by Gradl et al. [2]. The varying wall thicknesses have been included in Table 2. The thicknesses were measured with a digital slide caliper by taking an average of five measurements for each wall. The measurements exclude the curled or failed parts' value to better illustrate the deviation for the universally successful builds. The deviation ranged between +178/-152 μm and the mean from 0 to 25 μm for universally successful builds[2]. For a better understanding of the visual representation of the incomplete and failed builds, a side view of the wall thickness is added in the Appendix.





Recoater direction

Fig 1: L-PBF additively manufactured Inconel 718 feature build plate artifact sample.

Table 1: Machine overview from shared information of vendor build parameters.

ID	Machine Model Type	Layer Height (µm)	Recoater Type	Power (W)	Scan Speed (mm/s)	Energy Density (J/mm³)	Core Scan Strategy
1	EOS M400	40	Rubber	285	960	74.2	Stripes
2	EOS M280	40	Steel	-	-	-	Stripes
3	EOS M280	40	-	-	-	-	-
4	EOS M290	40	Carbide Knife	285	960	74.2	Stripes
5	EOS M280	40	Brush	285	960	74.2	Stripes
6	EOS M280	40	Soft Recoater	285	960	74.2	Stripes
7	Concept M2	30	Rubber	180	600	95.2	Checkered
8	EOS M280	40	High-Speed Steel	285	960	74.2	Stripes
9	EOS M290	40	EOS Steel	285	900	-	Stripes
10	SLM280	30	Silicone	200	900	61.7	Stripes
11	SLM280 Dual	30	Silicone	200	900	61.7	Stripes
12	Velo Sapphire	50	Non-Contact	_	-	-	Checkered
13	EOS M290	40	Carbon	285	960	74.2	Stripes
14	EOS M290	40	Steel	285	960	74.2	Stripes
15	EOS M280	40	Carbon Fiber Brush	285	960	74.2	Stripes
16	EOS M290	40	Carbon Fiber Brush	285	960	74.2	Stripes

Table 2: Varying Thicknesses of Vertical Thin Walls

		Per Specifications: Vertical Thin Walls, Varying Thicknesses (mm)								
Wall	1	2	3	4	5	6	7			
Nominal Thickness		0.10	0.20	0.41	0.61	0.81	1.02	2.03		
Machine	Build plate Identifier	Vertical Thin Walls, Varying Thicknesses (mm)								
EOS M400	1	0.22	0.32	0.46	0.64	0.83	1.02	2.04		
EOS M280	2	-	0.25	0.42	0.61	0.80	1.00	2.04		
EOS M280	3	-	0.19	0.36	0.55	0.74	0.97	1.98		
EOS M290	4	0.14	0.22	0.34	0.55	0.75	0.94	1.96		
EOS M280	5	-	0.28	0.43	0.61	0.83	1.02	2.03		
EOS M280	6	-	0.14	0.37	0.53	0.74	0.94	1.93		
Concept M2	7	0.22	0.33	0.39	0.44	0.79	1.05	2.13		
EOS M280	8	0.22	0.19	0.37	0.56	0.76	0.97	1.98		
EOS M290	9	-	0.29	0.42	0.61	0.84	1.02	2.03		
SLM280	10	0.20	0.24	0.39	0.61	0.83	1.02	2.03		
SLM280-Dual	11	0.22	0.36	0.36	0.55	0.80	0.95	2.04		
VELO Sapphire	12	0.19	0.17	0.30	0.58	0.77	0.98	2.03		
EOS M290	13	0.11	0.28	0.39	0.61	0.81	1.00	2.01		
EOS M290	14	0.14	0.20	0.38	0.58	0.80	0.99	2.02		
EOS M280	15	-	0.25	0.38	0.57	0.79	0.98	1.99		
EOS M290	16	0.14	0.25	0.43	0.62	0.83	1.02	2.03		
	,									
Average Deviation		0.08	0.05	0.03	0.04	0.03	0.02	0.03		
Average		0.11	0.25	0.38	0.58	0.79	0.99	2.02		
Standard Deviation		0.09	0.06	0.05	0.05	0.03	0.03	0.05		

2.2 Methods

Each build plate's varying thin wall part was removed via EDM. Thin wall samples were sectioned in XY and YZ axes by a BRILLIANT 220 abrasive cut-off machine. An OPAL 460 hot mounting press machine was used to mount the thin wall pieces. The mounted pucks were ground and polished via a SPHIR 530 twin-wheel grinder and polisher. Kalling's No. 2 Reagent (2g CuCl₂, 40 ml HCl, 40-80 ml Ethanol) was used to etch the polished samples. The sectioning and mounting of the thin wall parts from the build plate are shown in Fig 2. The optical microscopic images at

100x and 200x magnification of as-Polished and as-Etched samples were acquired on an OLYMPUS GX53 optical microscope.

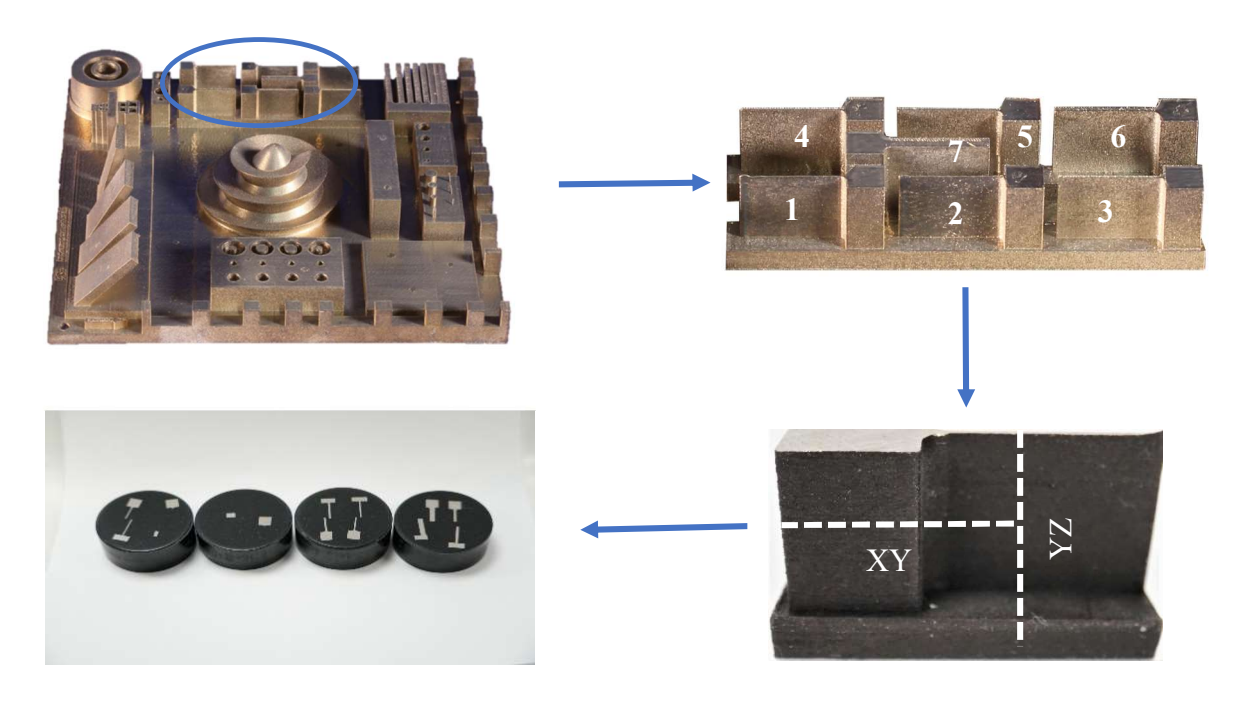


Fig 2: Sectioning and mounting of the thin wall parts.

2.3 Grain width measurements

The grain width measurements were calculated by the line intercept method, a process described in ASTM E112. ImageJ software was used to draw at least five straight lines (three lines parallelly and two diagonally) across the micrograph of 200x magnification at different angles for both XY and YZ planes and to count intercepted grain boundary numbers [6]. The average of five straight lines and five intersections were determined for each micrograph.

2.4 Equation

The average grain width for each XY and YZ plane of sixteen samples was measured using the following formula:

$$Average \ Grain \ size \ (microns) = \frac{Average \ length \ of \ the \ straight \ lines \ (microns)}{Average \ number \ of \ intersections} \tag{1}$$

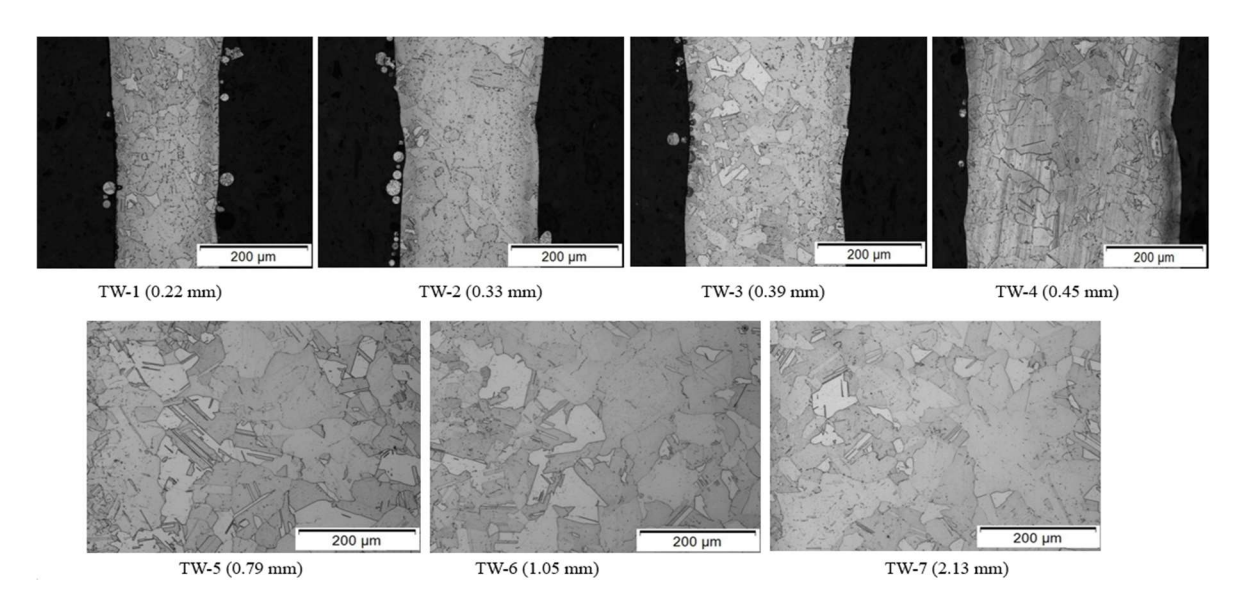
2.5 Micro-indentation Hardness Measurement

Micro-indentation Vickers hardness testing was completed across the length of the walls by a Qness 30 CHD Master⁺ Microhardness tester according to ASTM E384.

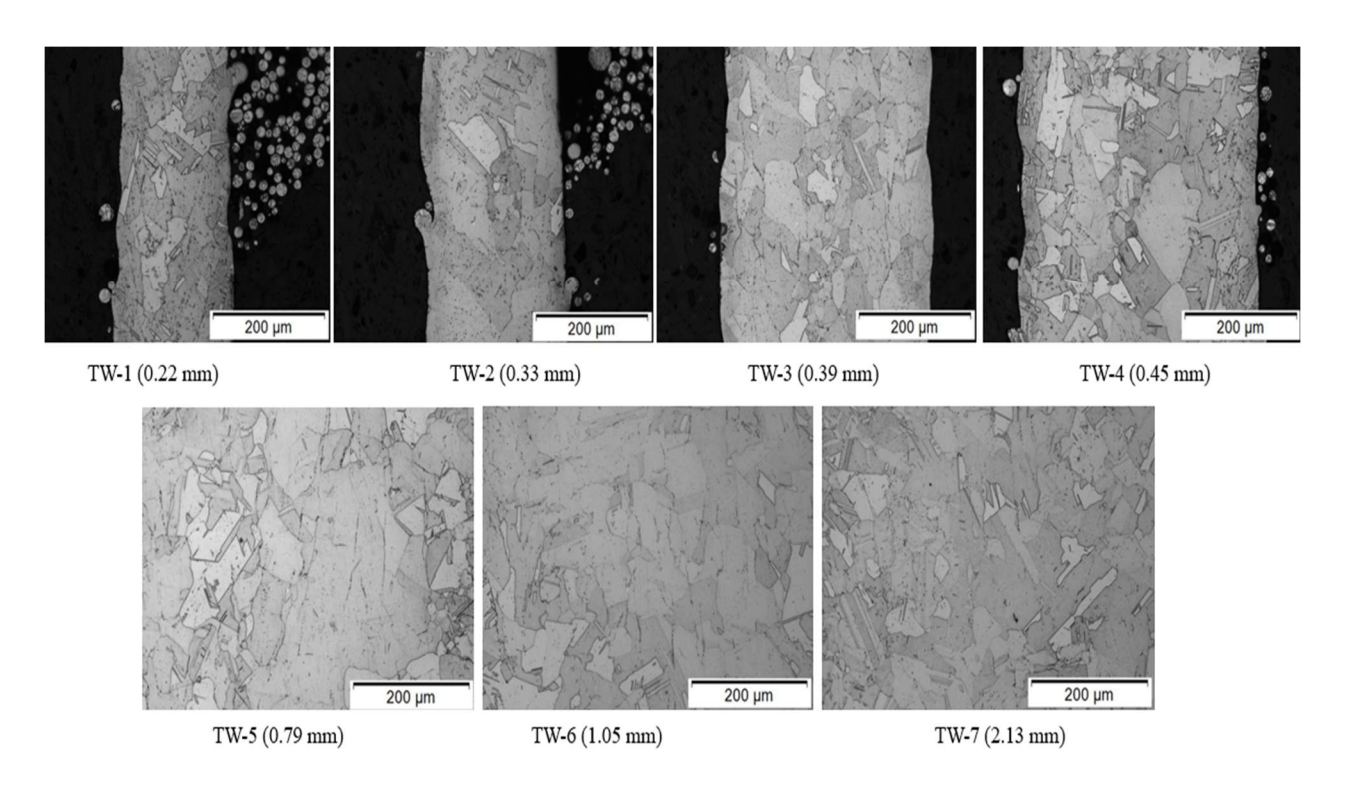
3 Results

This work presented here summarized fully heat-treated (SR, HIP, SOL, AGE) vertical thin wall samples (Sample 7,10,12, and 16) from four different machines (Concept M2, SLM 280, VELO Sapphire, and EOS M290) that have been evaluated with grain width measurement and Vickers microhardness testing. Figure 3 displays the etched micrographs of the thin wall samples for the XY and YZ planes. It can be seen from the micrographs that there are equiaxed grain sizes and a good number of twins across the walls. There is also precipitation with varying amounts in all the samples. Smaller grain sizes can be seen at the edge of the walls. The grains' size increases with the vertical walls' increasing thickness. The average grain width plot for samples 7,10,12, and 16 is shown in Figure 4. For the thinnest wall (Wall No. 1; 0.1 mm), the average grain width ranges from 21 to 46 microns; the thickest wall (Wall No. 7; 2 mm) ranges from 60 to 87 microns.

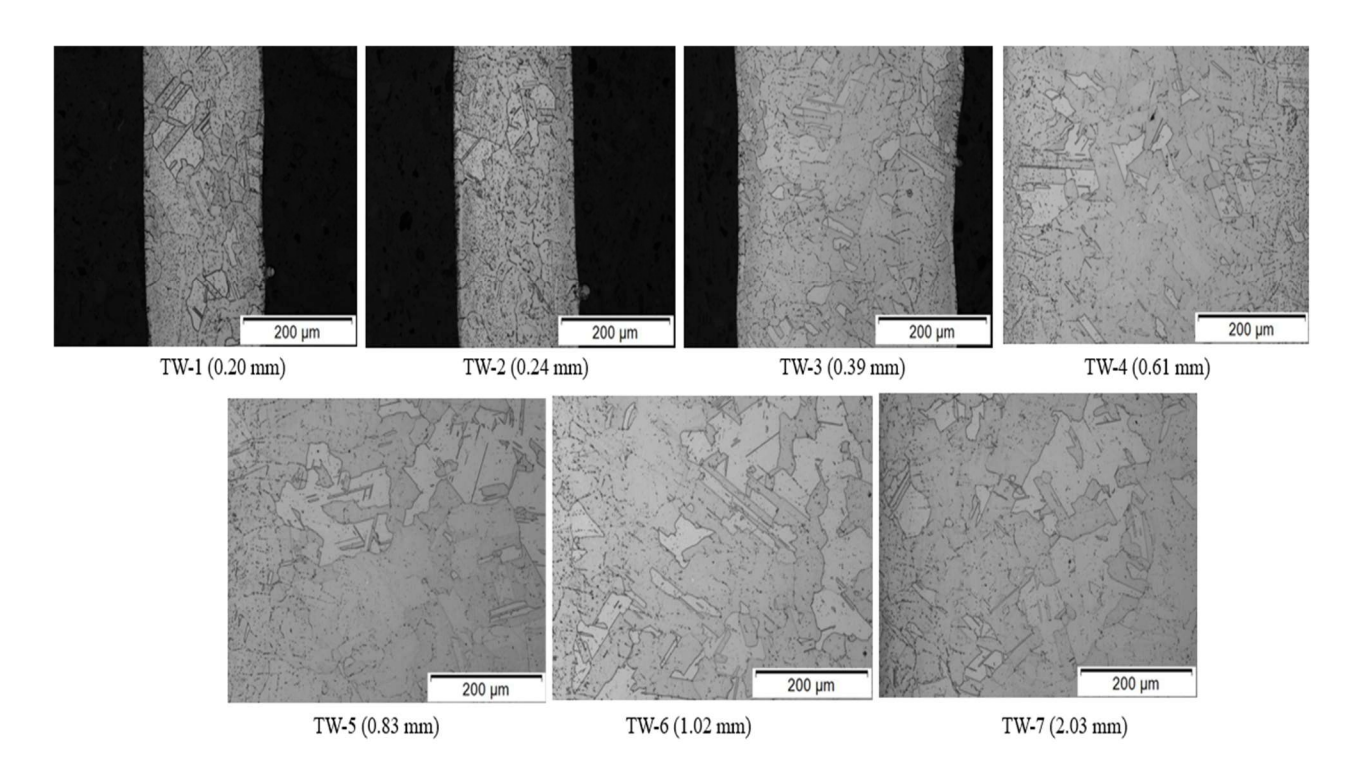
In the case of thin wall no.7 (2 mm) from all the samples, the average grain width plot is displayed in Figure 5. It is clearly seen from Figure 4 that grain size becomes larger with the increase in thickness of the walls, and the variation trend in grain size is similar for four samples (7,10,12, and 16) across four different machine platforms. The average grain size value (ranges from 60 to 95 microns) becomes more consistent with the thickest wall (No. 7; 2 mm), which is evidenced from Figure 5. Vickers microhardness plots, including varying wall thicknesses for samples 7,10,12, and 16, are shown in Figure 5. The microhardness value ranges from 388 HV to 467 HV for Wall No. 1 (0.1 mm) and 459 HV to 489 HV for Wall No. 7 (2 mm). With the same post-processing for all the samples, microhardness results show no significant variation for the four samples regardless of different machine platforms.



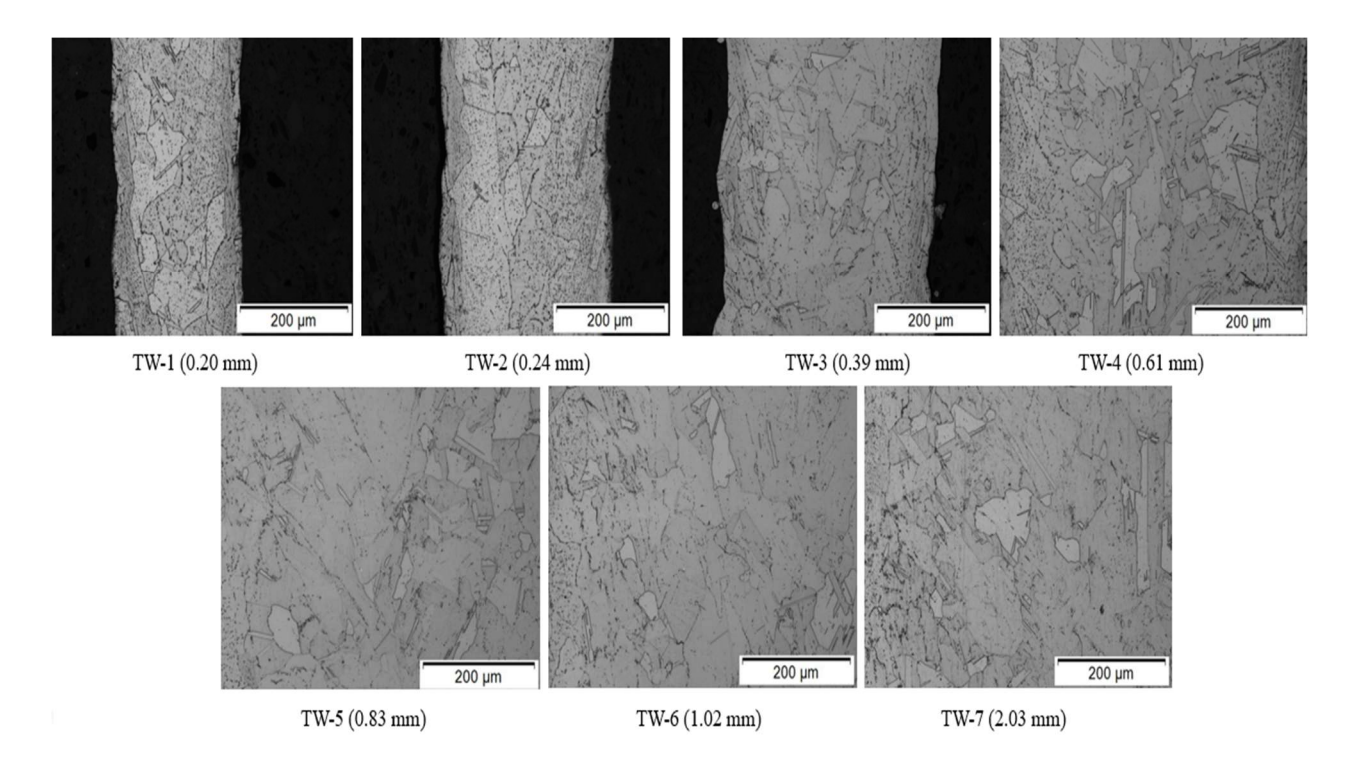
(a) Sample 7(XY), Concept M2.



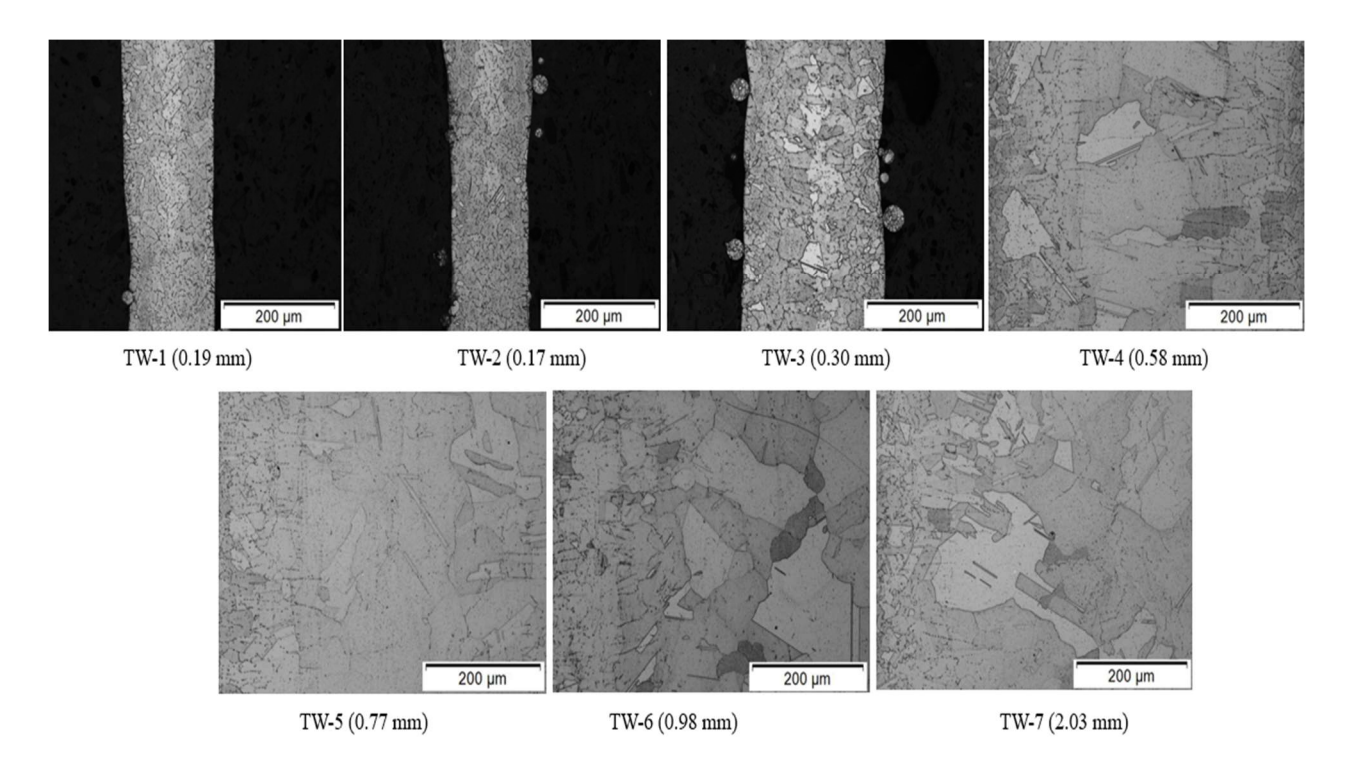
(b) Sample 7(XY), Concept M2.



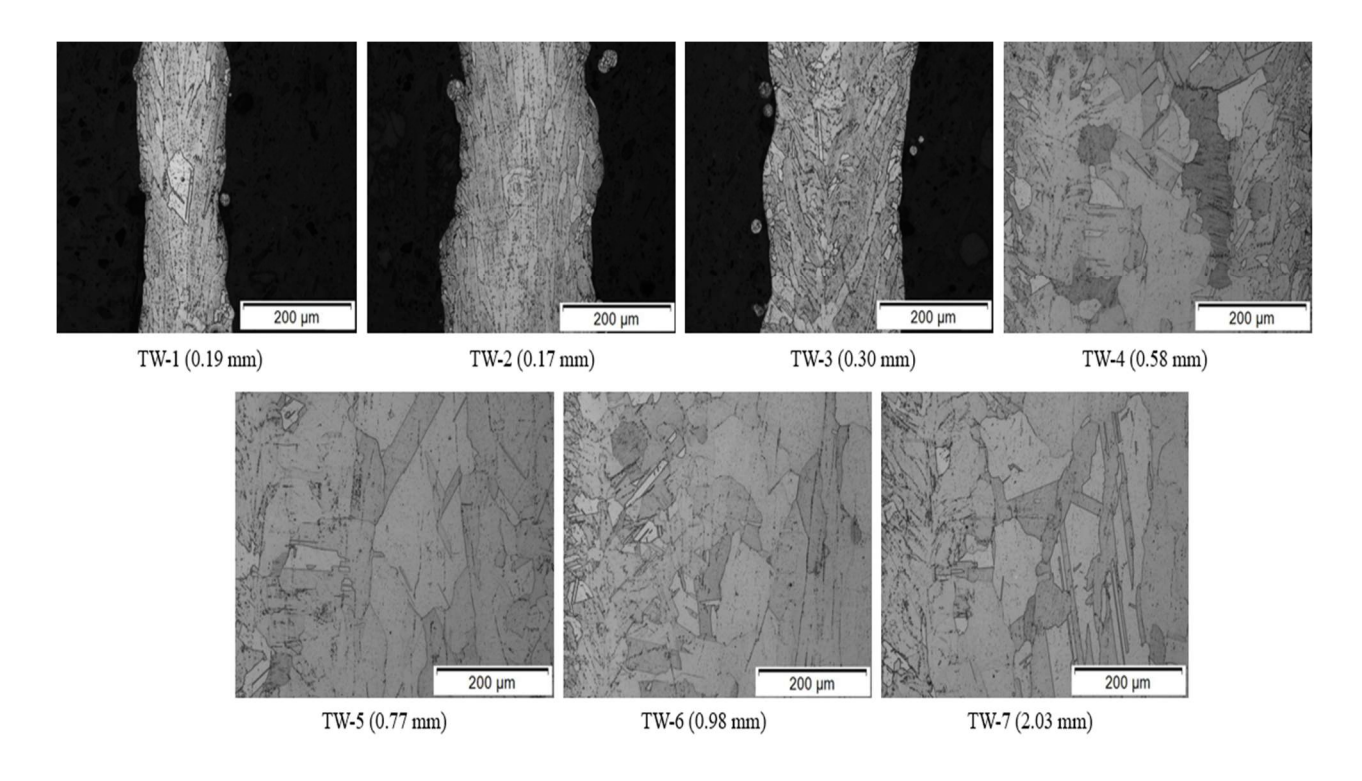
(c) Sample 10 (XY), SLM 280.



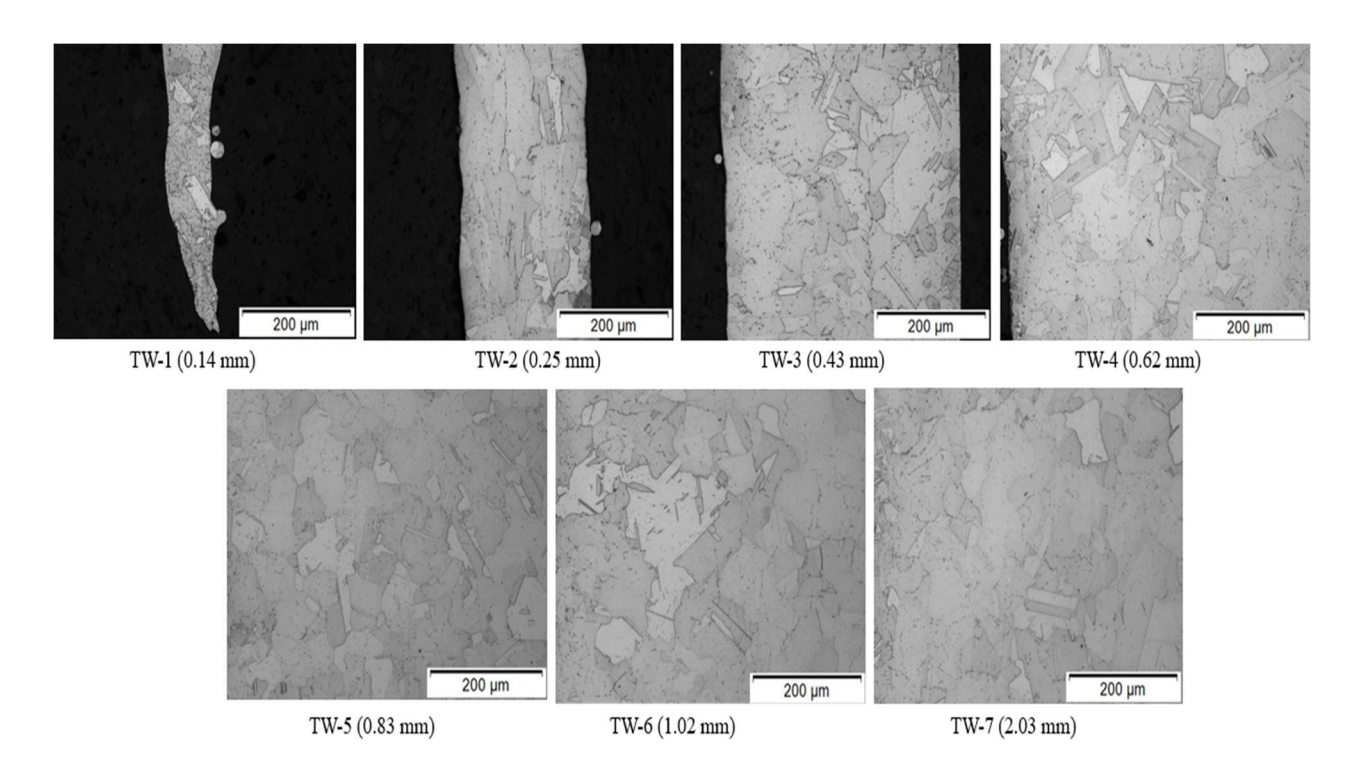
(d) Sample 10 (YZ), SLM 280.



(e) Sample 12 (XY), VELO Sapphire.



(f) Sample 12 (YZ), VELO Sapphire.



(g) Sample 16 (XY), EOS M290.

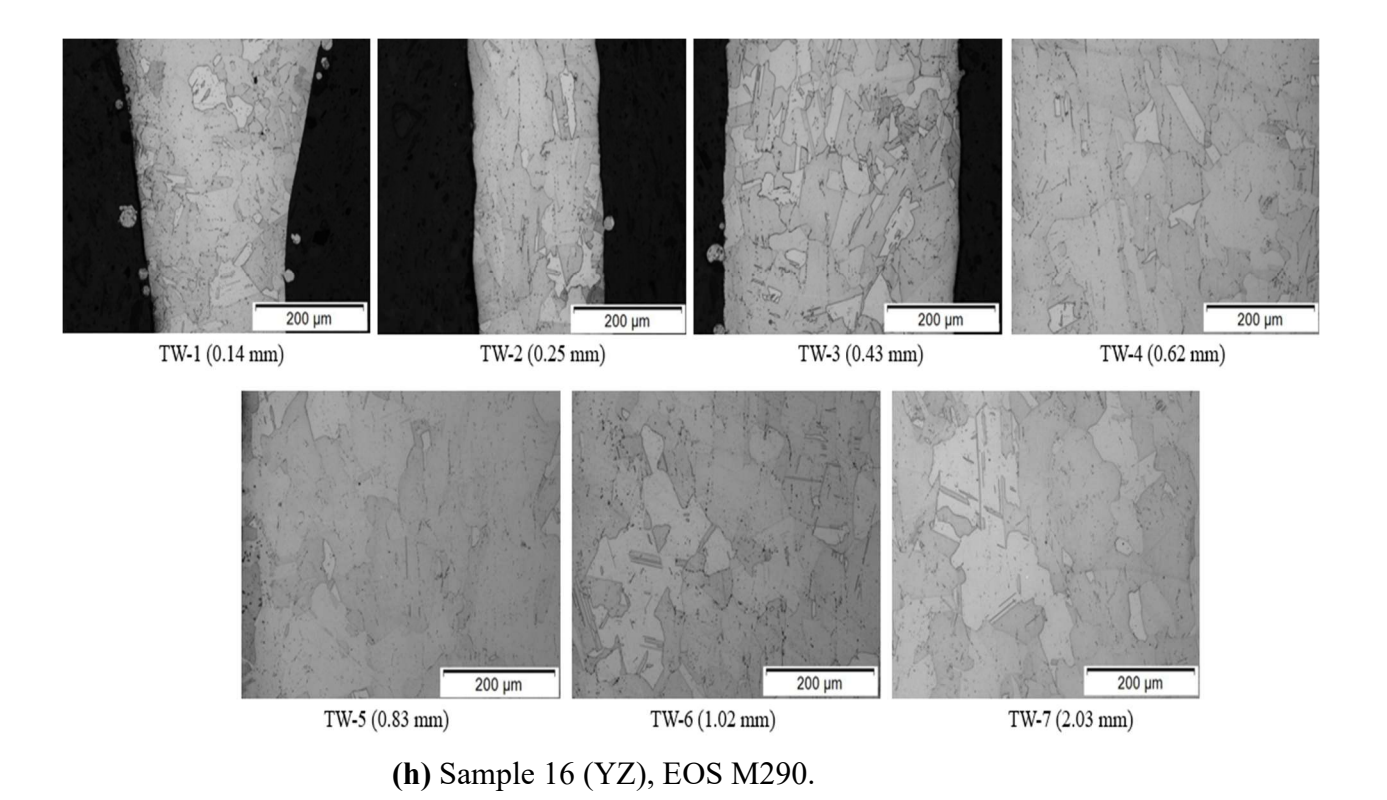


Fig 3: Etched Micrographs of Sample 7, 10, 12, & 16.

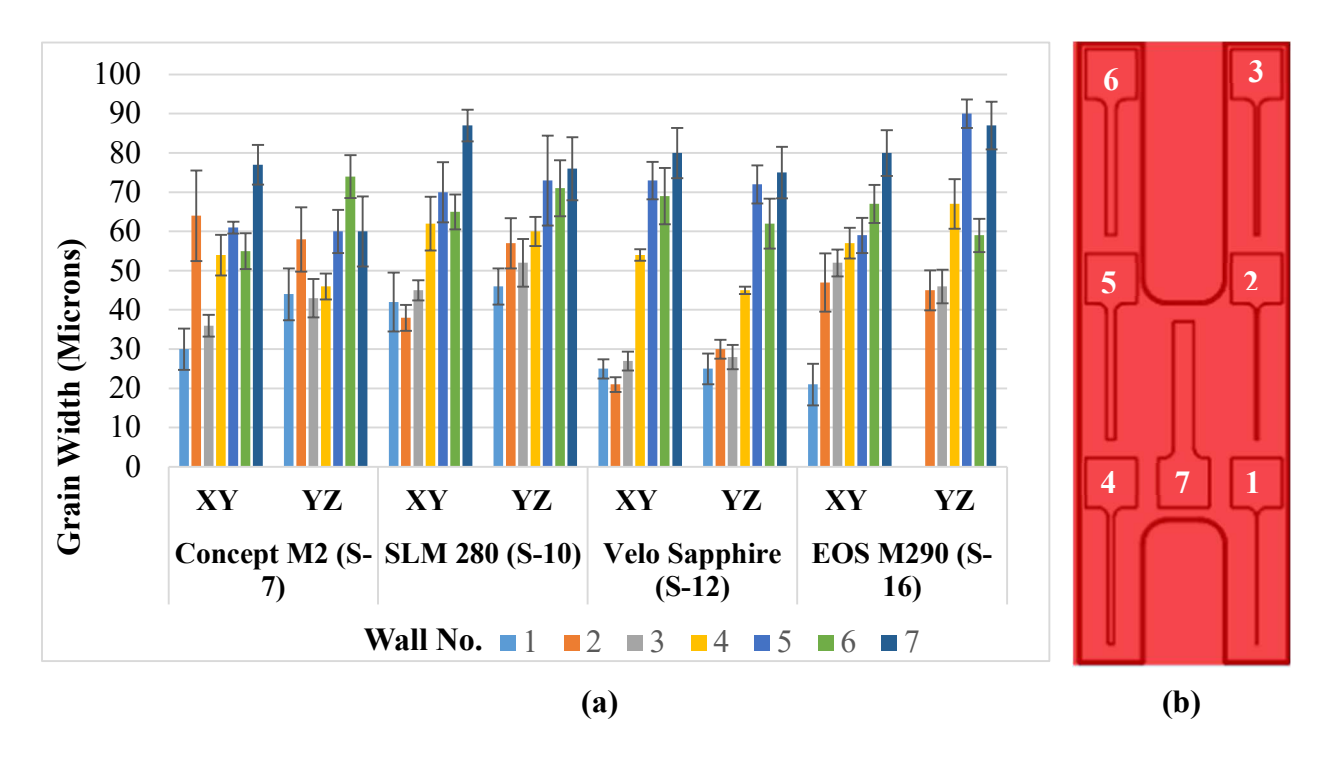


Fig 4: (a) Average Grain Width for Sample 7,10,12, & 16. (b) Schematic image of the thin wall specimen.

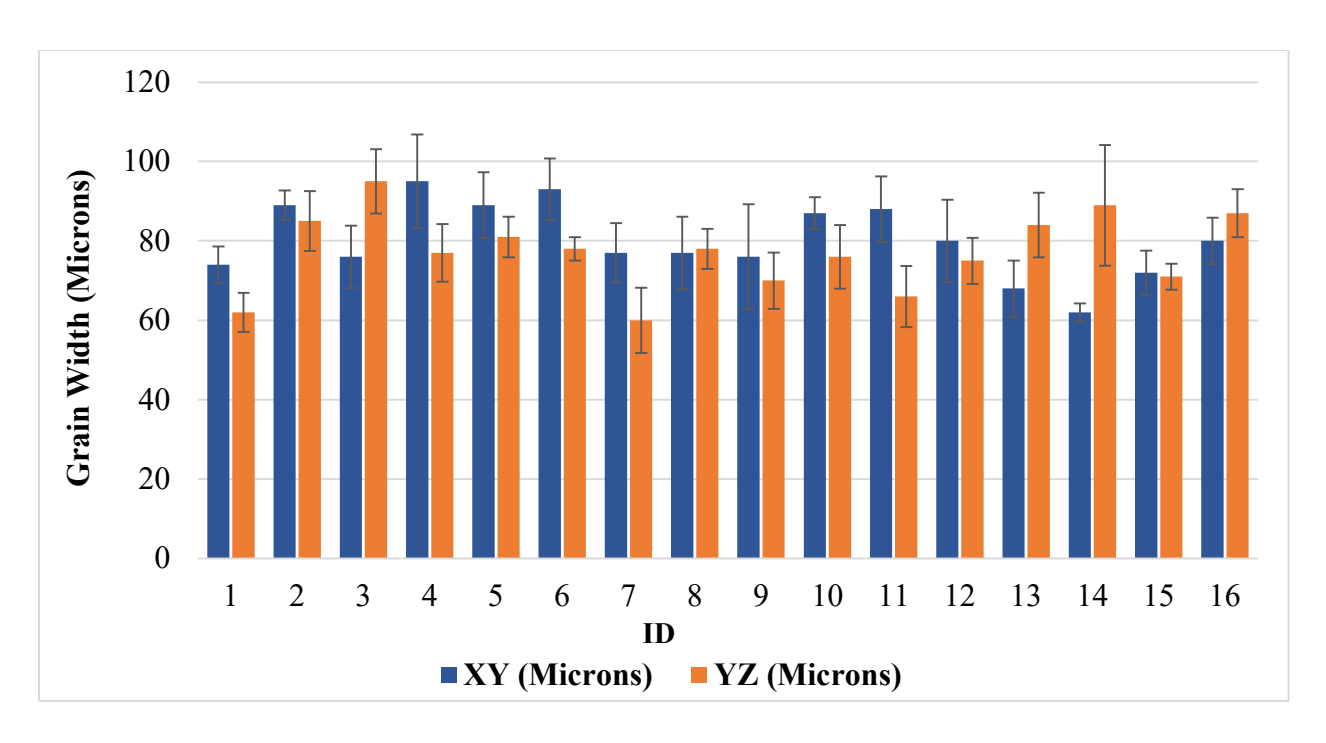


Fig 5: Average Grain Width for thin wall 7 from all sixteen samples.

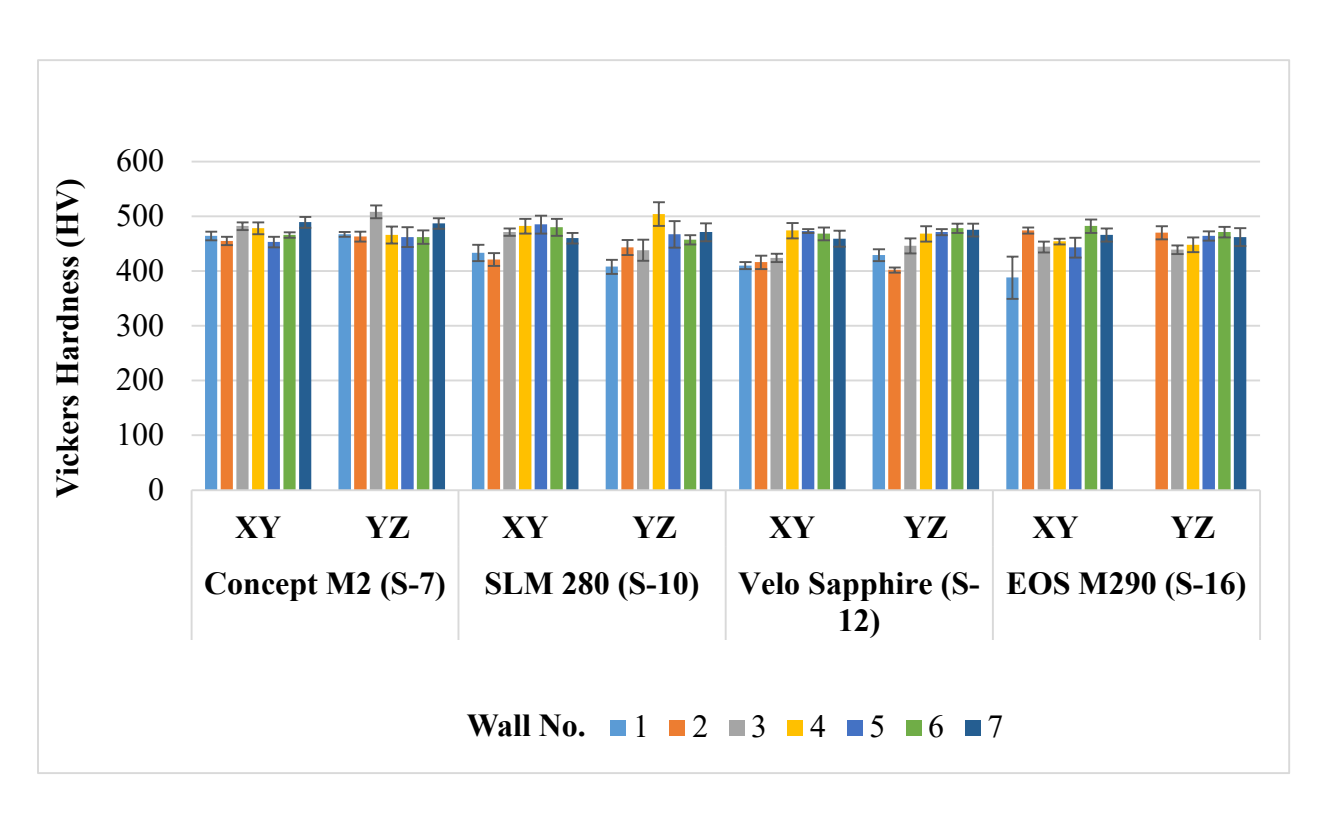


Fig 6: Vickers Microhardness Measurement.

4 Discussion

The current work presents the evidence that irrespective of different machine platforms, walls of varying thicknesses show analogous trends for the four L-PBF processed samples. No. 1 wall, which is the thinnest one (0.1 mm), has smaller grain sizes, while No. 7 wall (thickest wall, 2 mm) has greater grain sizes. While manufactured via L-PBF, layer-by-layer material deposition causes the material to undergo several thermal cycles. During a new layer deposition, the material from the previously deposited layer is re-melted partly and reheated, corresponding to high temperatures. This re-melting aids the grain growth from the preceding layer to the new one. With the increase in sample thickness, an additional number of laser passes increases the re-heating cycles. The thinner wall has undergone fewer re-heating cycles than the thicker one. Therefore, the average cooling rate is faster in thinner walls corresponding to thicker walls, which leads to smaller grain size. In the case of the thickest wall (No. 7, 2 mm), the average cooling rate is slower and more consistent due to increased thickness, which is a possible reason behind larger and not so varying grain sizes regardless of the different machines with minor parameter variations [6], [9], [10]

The analogous behavior of the microhardness values can lead to evidence that the specimen can achieve similar hardness results with the same properly applied heat treatments.

5 Conclusion

The present study analyzed the microstructure and microhardness properties for L-PBF additively manufactured Inconel 718 vertical thin walls with varying thicknesses from 0.1 to 2.0 mm. Regardless of different machine platforms, the grain width is shown to increase proportionally with the thickness of the wall. The grain size shows an upward trend with the increased thickness. The increase in laser deposition along with thickness can lead to a lower average cooling rate and larger grain sizes. The thickest wall (No.7; 2 mm) has a larger grain size with a more consistent value for four samples from different machine manufacturers. Smaller grain size can lead to higher strength according to the Hall-Petch relationship [11]. However, the thinner wall specimen can be subjected to the greater effect of defects, which can lead to lower strength despite smaller grain size. In the case of microhardness, values fall into a narrower range (~400 to 500 HV). A possible reason can be undergoing the same full heat-treatment (post-processing) irrespective of different machine platforms.

This is an ongoing project. Future work will include microstructure and microhardness properties evaluation of all the sixteen samples from fifteen different machines. Further work will compare the microstructure and microhardness properties of as-built and HIP-ed built parts with the fully post-processed ones to evaluate the importance of heat-treatment on the L-PBF processed Inconel 718 thin walls. This study will be helpful for designers to be informed about how machine parameters, configurations, and correct post-processing could result in similar properties but potential variations based on the thickness of features.

Acknowledgments

The research described here was performed at The University of Texas at El Paso (UTEP) within the W.M. Keck Center for 3D Innovation (Keck Center). Primary support for this research was provided by Grant Number 80NSSC22PA055 from NASA, Rapid Analysis and Manufacturing of Propulsion Technology. Additional strategic investments were provided via discretionary UTEP Keck Center funds and the Mr. and Mrs. MacIntosh Murchison Chair I in Engineering Endowment at UTEP. The views and opinions expressed in this article are those of the authors and do not necessarily reflect the official opinion or policy of NASA.

Appendix

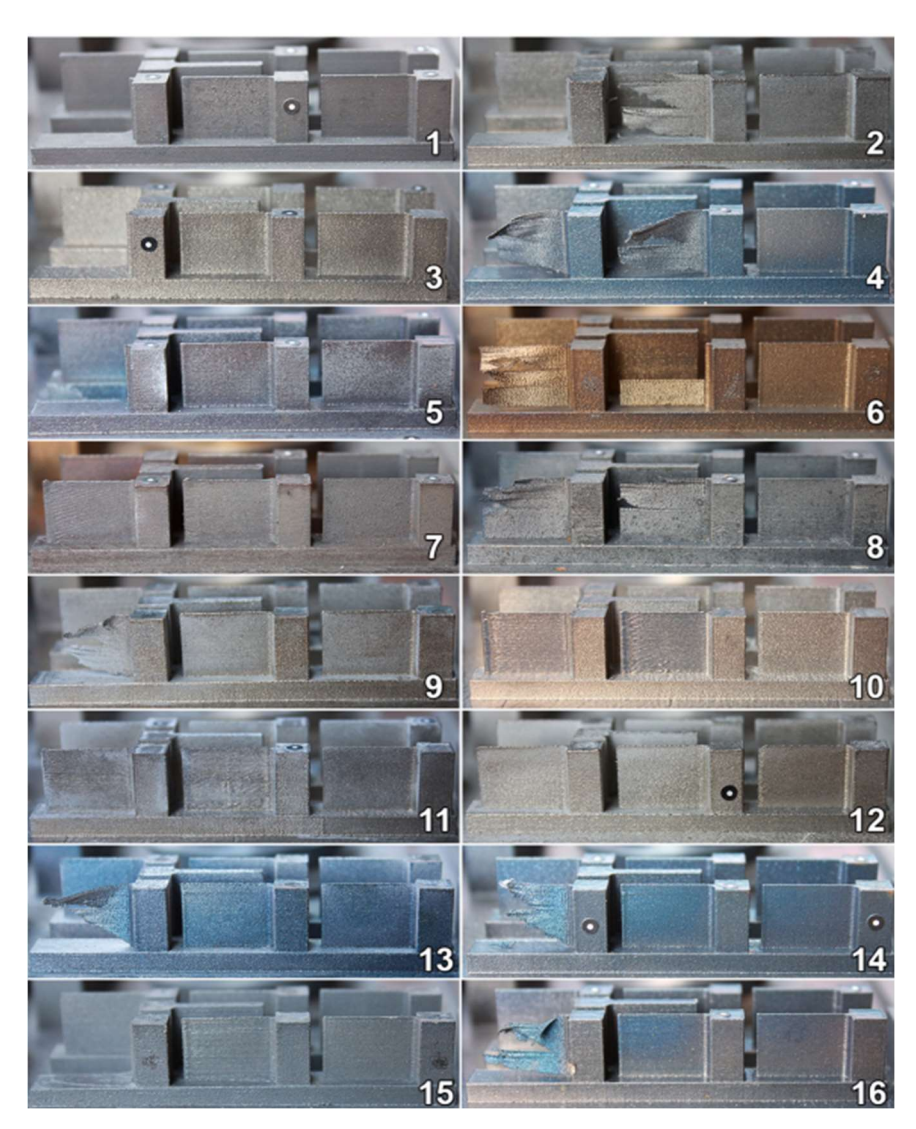


Fig 7: Failed wall thickness at 0.10 and 0.20 mm for all machine configurations.

References

- [1] P. Gradl *et al.*, "Robust Metal Additive Manufacturing Process Selection and Development for Aerospace Components," *J Mater Eng Perform*, 2022, doi: 10.1007/s11665-022-06850-0.
- [2] P. R. Gradl, D. C. Tinker, J. Ivester, S. W. Skinner, T. Teasley, and J. L. Bili, "Geometric feature reproducibility for laser powder bed fusion (L-PBF) additive manufacturing with Inconel 718," *Addit Manuf*, vol. 47, Nov. 2021, doi: 10.1016/j.addma.2021.102305.
- [3] B. Blakey-Milner *et al.*, "Metal additive manufacturing in aerospace: A review," *Mater Des*, vol. 209, p. 110008, 2021, doi: https://doi.org/10.1016/j.matdes.2021.110008.
- [4] M. Leary, "Powder bed fusion," in *Design for Additive Manufacturing*, Elsevier, 2020, pp. 295–319. doi: 10.1016/b978-0-12-816721-2.00011-7.
- [5] J. P. Oliveira, A. D. Lalonde, and J. Ma, "Processing parameters in laser powder bed fusion metal additive manufacturing 193 (2020) 1–12." 2020.
- [6] S. Y. Ahn *et al.*, "Thickness effect on the microstructures, mechanical properties, and anisotropy of laser-powder bed fusion processed 316L stainless steel," *J Mater Sci*, Jul. 2022, doi: 10.1007/s10853-022-07516-x.
- [7] H. C. Chen, A. J. Pinkerton, and L. Li, "Fibre laser welding of dissimilar alloys of Ti-6Al-4V and Inconel 718 for aerospace applications," *International Journal of Advanced Manufacturing Technology*, vol. 52, no. 9–12, pp. 977–987, Feb. 2011, doi: 10.1007/s00170-010-2791-3.
- [8] C. A. Schneider, W. S. Rasband, and K. W. Eliceiri, "NIH Image to ImageJ: 25 years of image analysis," *Nat Methods*, vol. 9, no. 7, pp. 671–675, Jul. 2012, doi: 10.1038/nmeth.2089.
- [9] J. Schneider *et al.*, "Microstructure Evolution in Inconel 718 Produced by Powder Bed Fusion Additive Manufacturing," *Journal of Manufacturing and Materials Processing*, vol. 6, no. 1, Feb. 2022, doi: 10.3390/jmmp6010020.
- [10] A. Gamon *et al.*, "Microstructure and hardness comparison of as-built inconel 625 alloy following various additive manufacturing processes," *Results in Materials*, vol. 12, p. 100239, Dec. 2021, doi: 10.1016/j.rinma.2021.100239.
- [11] A. Robbins, "Mechanical Characterization of Additively Manufactured Inconel Mechanical Characterization of Additively Manufactured Inconel 625 and AlSi10Mg via High-Throughput Tensile Testing 625 and AlSi10Mg via High-Throughput Tensile Testing."

 [Online]. Available: https://digitalrepository.unm.edu/me_etds/177